Chemical Engineering Journal 519 (2025) 164905

Contents lists available at ScienceDirect

Chemical Engineering Journal

journal homepage: www.elsevier.com/locate/cej

From AI to action: Antimicrobial peptides engineered by generative adversarial networks (GANs)-A novel approach to combat resistant Bacteria

Chia-Wen Lai [a,1], Chung-Yen Lin [b,c,1], Meng-Chen Tsai [a], Wei-Jung Chen [d], Chia-Chun Hsieh [e], Zi-Jing Lin [e], Li-Jiuan Shen [f,g,h], Ying-Lien Chen [i], Lee-Jene Lai [e], Shu-Hwa Chen [j,*], Yang-Hsin Shih [a,*]

[a] Department of Agricultural Chemistry, National Taiwan University, No. 1, Sec. 4, Roosevelt Rd., Taipei 10617, Taiwan
[b] Institute of Information Science, Academia Sinica, No. 128, Sec. 2, Academia Road, Nankang, Taipei 11529, Taiwan
[c] Institute of Fisheries Science, National Taiwan University, No. 1, Sec. 4, Roosevelt Rd., Taipei 10617, Taiwan
[d] Department of Biotechnology and Animal Science, National Ilan University, No.1, Sec. 1, Shennong Rd., Yilan City, Yilan County 26047, Taiwan
[e] National Synchrotron Radiation Research Center, No. 101 Hsin-Ann Road, Hsinchu Science Park, Hsinchu 300092, Taiwan
[f] School of Pharmacy, National Taiwan University, No.33, Linsen S. Rd., Zhongzheng Dist., Taipei City 100025, Taiwan
[g] Graduate Institute of Clinical Pharmacy, College of Medicine, National Taiwan University, No.33, Linsen S. Rd., Zhongzheng Dist., Taipei City 100025, Taiwan
[h] Department of Pharmacy, National Taiwan University Hospital, No.33, Linsen S. Rd., Zhongzheng Dist., Taipei City 100025, Taiwan
[i] Department of Plant Pathology and Microbiology, National Taiwan University, No. 1, Sec. 4, Roosevelt Rd., Taipei 10617, Taiwan
[j] TMU Research Center of Cancer Translational Medicine, Taipei Medical University, No. 250 Wu-Hsing St., Taipei 11031, Taiwan

ARTICLE INFO

Keywords:
Antimicrobial peptides
Generative adversarial network
Resistant bacteria
AI-designed

ABSTRACT

With the growing threat of antibiotic-resistant bacteria, the need for innovative antibacterial treatments is more urgent than ever. Antimicrobial peptides (AMPs) are gaining attention due to their unique mechanisms of action. We utilized a Wasserstein generative adversarial network (WGAN) with a gradient penalty to expedite the discovery of new AMP candidates. Among the promising peptides identified, GAN-pep3 stood out with its impressive antibacterial activity against Gram-negative and Gram-positive bacteria. It achieved a low geometric mean minimum inhibitory concentration (MIC) of 0.90 μM and 4.21 μM, respectively. Although GAN-pep3 showed slight hemolytic activity, its low MIC provided a high therapeutic index, particularly against Gram-negative bacteria. This study highlights the potential of AI-designed AMPs as powerful antimicrobial agents with broad-spectrum activity. It instills hope for significant therapeutic applications in the fight against antibiotic-resistant bacteria.

1. Introduction

Antimicrobial resistance (AMR) occurs when microbes evade antibiotics that were once effective against them. Microbes with antimicrobial resistance (AMR) properties continue to grow, making conventional treatment strategies ineffective [1–3]. Insufficient antibiotic dosing, non-compliance with medical treatment protocols, and the excessive or improper use of antibiotics in agriculture and livestock operations contribute to the selection pressure that favors antibiotic-resistant microbes [3,4]. Given the time-consuming and costly nature of discovering new antibiotics and the challenges associated with scaling up production through purification or de novo synthesis, it is imperative to develop new strategies to combat microbial threats in human medical care and veterinary medicine.

Antimicrobial peptides (AMPs) are found in various species and typically consist of 6 to 50 amino acids. They are known for their ability to eliminate microbes and are being studied as potential candidates for a new class of antibiotic agents [5,6]. AMPs are part of the host's innate immune response against bacteria, fungi, viruses, and cancer cells [7]. Discovering novel antimicrobial peptides (AMPs) typically involves collecting these peptides from various organisms, which often requires significant time and financial investments [8]. The mechanism of target killing by AMPs involves peptide aggregation on the cell surface, which ultimately causes membrane rupture [9–13]. For clinical applications,

* Corresponding authors.
E-mail addresses: sophia0715@tmu.edu.tw (S.-H. Chen), yhs@ntu.edu.tw (Y.-H. Shih).
[1] The joint first authors.

https://doi.org/10.1016/j.cej.2025.164905
Received 26 November 2024; Received in revised form 24 May 2025; Accepted 13 June 2025
Available online 15 June 2025

antimicrobial peptides (AMPs) must distinguish effectively between bacterial and host cell membranes to avoid cytotoxicity in mammalian cells, a challenge often seen with cationic AMPs [14].

To accelerate the discovery of novel antimicrobial peptides (AMPs), we employed a deep learning framework based on generative adversarial networks (GANs) [15–17]. Our initial efforts utilized a deep convolutional GAN (DCGAN) trained on known AMP sequences. However, to overcome the limitations of training instability and mode collapse inherent in the original GAN architecture, we implemented the Wasserstein GAN with Gradient Penalty (WGAN-GP). This enhanced architecture provides improved stability, enabling the model to learn key sequences and physicochemical features more effectively, critical to AMP activity. The WGAN-GP model was trained on encoded AMP sequences and generated novel peptide candidates from random noise inputs.

In our previous study [18], we validated the model's generative performance by comparing the amino acid composition and eight physicochemical properties, including charge, hydrophobicity, Boman index, and aliphatic index, of GAN-designed peptides with those of real AMPs, randomly shuffled sequences, and helical controls. As shown in Figs. 1–3 of that study, the GAN-designed peptides closely mirrored real AMPs in both sequence and property distribution. t-SNE analysis further confirmed that GAN-generated peptides clustered closely with real AMPs and distinctly from control sequences, highlighting the model's ability to generate AMP-like molecules in silico.

Building on these findings, we applied an AI-guided screening pipeline using AI4AMP (http://axp.iis.sinica.edu.tw/AI4AMP), an *in-silico* AMP activity predictor developed by our team, to prioritize candidates with high predicted antimicrobial potential. Of the eight top-scoring peptides synthesized, seven demonstrated in vitro antimicrobial activity. Among them, GAN-pep 3 and GAN-pep 8 exhibited broad-spectrum efficacy, including activity against methicillin-resistant *Staphylococcus aureus* (MRSA) and carbapenem-resistant *Pseudomonas aeruginosa* (CRPA). Notably, GAN-pep 3 showed superior potency, with lower MIC values, compared to the positive control Polyphemusin I. Together, these results support the use of WGAN-GP as a robust platform for the rational and efficient design of next-generation AMPs with therapeutic potential against antibiotic-resistant pathogens [18,19].

In this study, the goals included assessing how the synthetic AMP sequence affected the growth and reproduction of both Gram-positive and Gram-negative bacteria, such as methicillin-susceptible *Staphylococcus aureus* (MSSA) and methicillin-resistant *Staphylococcus aureus* (MRSA), as well as *Escherichia coli* (*E. coli*), carbapenem-susceptible *Pseudomonas aeruginosa* (CSPA), and carbapenem-resistant *Pseudomonas aeruginosa* (CRPA). In addition, the antimicrobial action of AMPs was validated by scanning electron microscopy (SEM), confocal laser scanning microscopy (CLSM), and cryo-soft X-ray tomography (Cryo-SXT). Furthermore, hemolyticity was examined by assessing the effects of the synthesized AMPs on red blood cells in vitro. This work investigates the antimicrobial properties and in vitro effects of these peptides, providing new insights into their potential as innovative therapeutic agents.

2. Materials and methods

2.1. Reagents and bacterial strains

Sodium bicarbonate (CAS No. 144-55-8, $NaHCO_3$), sodium phosphate dibasic (CAS No. 7558-79-4, Na_2HPO_4), sodium phosphate monobasic (CAS No. 7558-80-7, NaH_2PO_4), glutaraldehyde (CAS No. 111-30-8, grade I), 4′,6-diamidino-2-phenylindole (CAS No. 28718-90-3, DAPI), propidium iodide (CAS No. 25535-16-4, PI), and lipopolysaccharide (LPS) from *Escherichia coli* serotype O111:B4 were purchased from Sigma-Aldrich (USA). Potassium chloride (CAS No. 7447-40-7, KCl), dodecyl sulfate sodium salt (CAS No. 151-21-3, SDS), and 2,2,2-trifluoroethanol (CAS No. 75-89-8, TFE) were purchased from Acros Organics (Belgium). Potassium phosphate monobasic (CAS No. 7778-77-7, KH_2PO_4) was purchased from Riedel-de Haën (Germany). Agar (CAS No. 9002-18-0), bio-tryptone (CAS No. 91079-40-2), and yeast extract (CAS No.8013-01-2) were purchased from BioShop (Canada). Sodium chloride (CAS No. 7647-14-5, NaCl) was purchased from Honeywell (Germany). Ethanol (CAS No. 64-17-5, EtOH) was purchased from Echo Chemical Co., Ltd. (Taiwan). *E. coli* (SG13009) is a strain with an RG grade of 1, which is derived from *E. coli* K12. Four clinical bacterial isolates, including methicillin-susceptible *S. aureus* (MSSA; S01-10-0202), methicillin-resistant *S. aureus* (MRSA; N07-10-0043), carbapenem-susceptible *P. aeruginosa* (CSPA; S07-10-0059), and carbapenem-resistant *P. aeruginosa* (CRPA; M06-06-0213), were screened from the

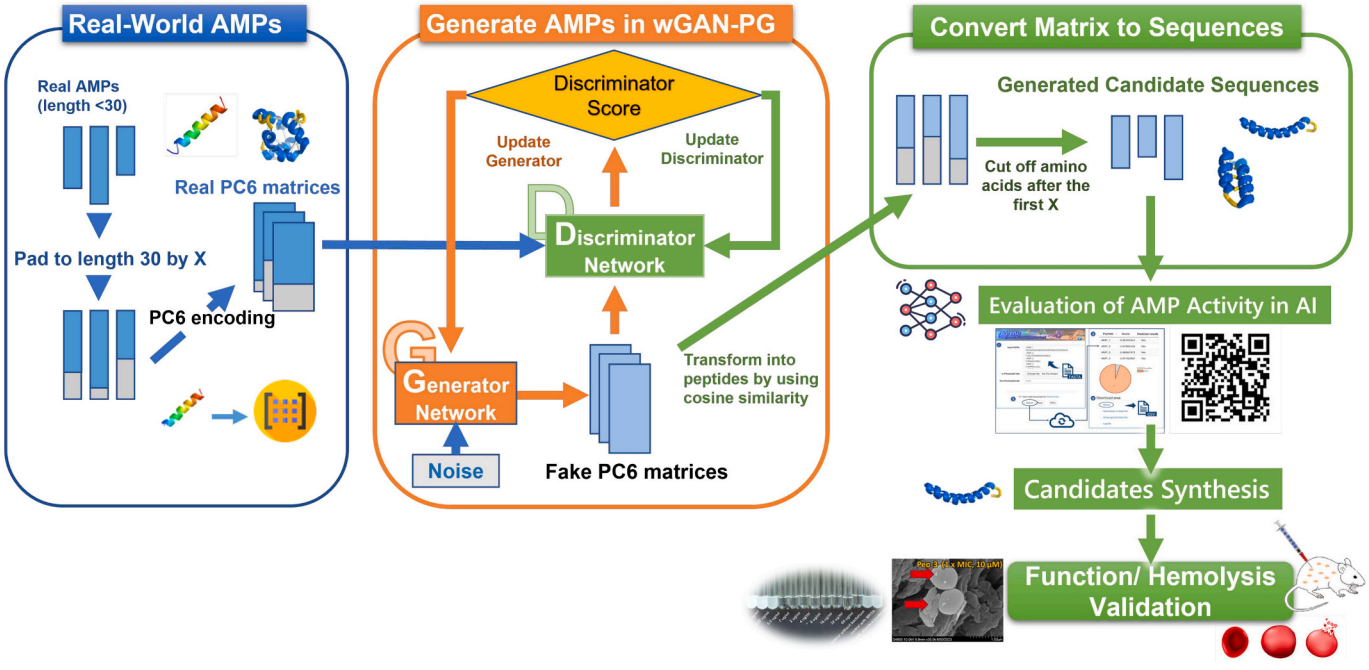

Fig. 1. Workflow of WGAN-PG model for training to generate and validate AMPs.

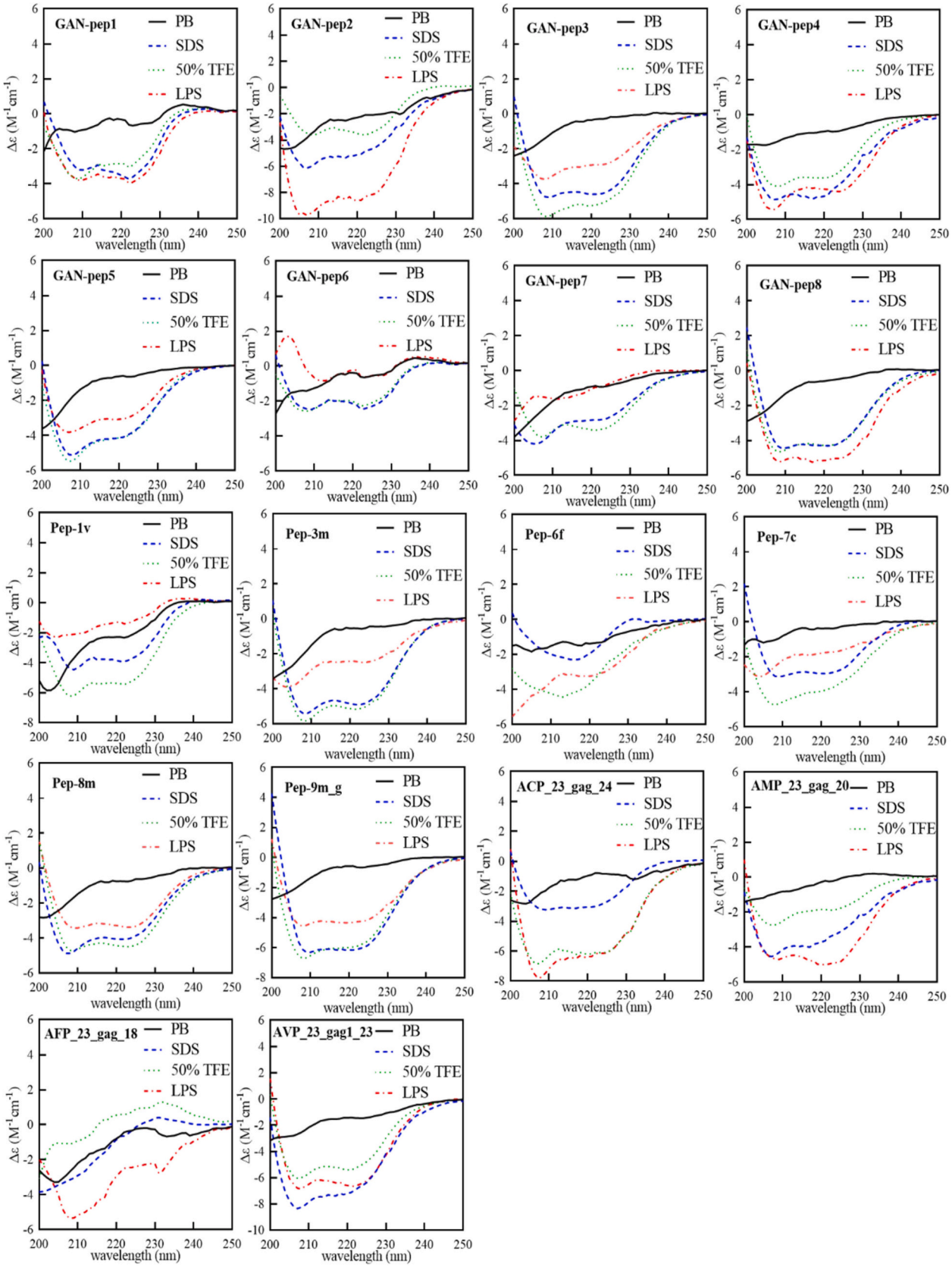

Fig. 2. CD spectra of peptides in different environments. AMPs were dissolved in 10 mM PB, 10 mM SDS, 50% TFE, and 20 μM LPS.

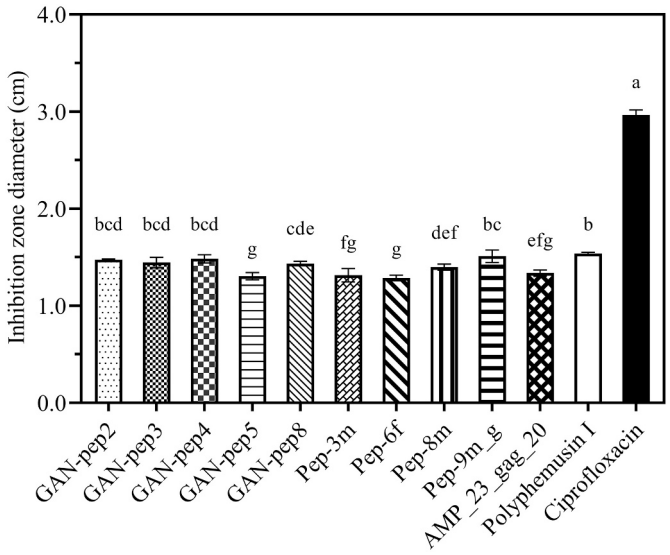

Fig. 3. Zone of inhibition introduced by 500 μg/mL of peptides and ciprofloxacin against *E. coli* cell (1.0×10^8 cfu/mL) after 18 h. Error bars represent the standard deviation of three repeated measurements. Groups labeled with different small letters (a, b, c, d, e, f, and g) indicate significant differences ($p < 0.05$) among treatments. Please refer to the legend for the specific grouping of each category.

Taiwan Surveillance of Antimicrobial Resistance (TSAR) program [20,21]. The bacteria used in this study were as follows. Microorganisms were cultured and propagated according to standard protocols. The stocks of bacteria were stored at −80 °C. All strains were grown aerobically at 37 °C in sterile Luria-Bertani (LB) media.

2.2. Peptide designed by the generative adversarial network (GAN)

The AMP candidates used in this study were generated from the prediction model published [18]. All data on AMPs were collected from four AMP databases [22–25]. Peptides with fewer than 10 amino acids or containing uncommon amino acids, including Asx (B), Xle (J), Pyl (O), Sec (U), Glx (Z), or Unk (X), were excluded from consideration. Due to the challenges and high costs associated with synthesizing longer peptides, only those with fewer than thirty amino acids were selected. A collection of 3195 AMPs was assembled to build and validate the model.

The fundamental architecture of GAN includes a discriminator and a generator [26]. The discriminator aims to differentiate between real data and artificial data created by the generator. The generator, conversely, attempts to produce artificial data that can deceive the discriminator. To enhance performance, the discriminator is updated to maximize its score for real data and minimize its score for artificial data. On the other hand, the generator is updated to maximize the discriminator's score for the artificial data it generates. The proposed GAN model for generating AMPs is based on DCGAN, a convolutional network-based GAN [15]. Convolution-transpose and convolution layers' kernel size, stride, and padding parameters were modified to suit the dimensions of the data better. To prevent mode collapse, the method outlined in WGAN-GP was employed [18]. Fig. 1 shows the entire process of training the GAN to produce AMPs.

2.3. The physicochemical properties of peptides

Mission Biotech (Taiwan) generated peptides with a purity exceeding 95% through traditional solid-phase peptide synthesis. The vendor supplied data on peptides characterized by mass spectrometry and high-performance liquid chromatography. All peptides were stored in a −80 °C refrigerator in powder form and then dissolved in sterile water before use in experiments. The net charge (eV) and percentage of hydrophobicity of peptides are calculated using a peptide property calculation provided by Peptide 2.0 Inc. (https://www.peptide2.com/).

2.4. Circular dichroism spectroscopy

The peptide secondary structure in the solution was determined using circular dichroism (CD) spectroscopy. The CD spectra of peptides were measured on a spectropolarimeter (Jasco, K-815, Tokyo, Japan). The spectra were captured using a time constant of 1 s, scanning at a rate of 50 nm/min and an interval of 1 nm, spanning a wavelength range from 250 to 200 nm. For CD measurement, 10 μM of peptides was in 10 mM phosphate buffer (PB), 10 mM sodium dodecyl sulfate (SDS), 50% trifluoroethanol (TFE), and 20 μM lipopolysaccharide (LPS), respectively. The BeStSel web server (https://bestsel.elte.hu/) calculates the secondary structures of peptides such as α-helix, parallel, anti-parallel, turn, and others. It offers a beta structure selection technique for evaluating the CD spectra generated by synchrotron radiation and conventional CD equipment [27].

2.5. Zone of inhibition

A well-diffusion technique was employed to test the antimicrobial activity against *E. coli* on LB agar. Paper discs (100% cotton fiber, Mini Trans-Blot®, Bio-Rad, USA) with a diameter of 6.3 mm were sterilized before use. 100 μL of diluted bacteria suspensions (1.0×10^8 colony-forming units per milliliter, or cfu/mL) was applied to the surface of the plate to solidify. After the paper discs were put on LB plates, 40 μL of 500 μg/mL peptide solution was added to each disc. The sizes of inhibition zones were measured by ImageJ (version 1.53a, National Institutes of Health, Bethesda, MD, USA) after incubation at 37 °C for 18 h. All experiments were performed in triplicate.

2.6. Minimum inhibitory concentration and minimum bactericidal concentration

The National Committee for Clinical Laboratory Standards (NCCLS) modified technique was used to estimate the minimum inhibitory concentration (MIC) of peptides against different bacterial strains [27]. Bacteria were inoculated at 37 °C in LB broth. Through UV–vis monitoring of the optical density (OD) at 600 nm (OD_{600}), the growth phase of bacteria was determined. The bacteria were diluted with LB broth to 10^5 cfu/mL as the final concentration. A 96-well plate (Cat # 269620, Thermo Fisher Scientific, Waltham, MA, USA) included 180 μL of the bacteria cells in each well, along with 20 μL of peptide solution that had been serially diluted with sterile water from 64 μg/mL. The peptide-free solution served as the positive control, while the bacterial-free LB broth was used as the negative control. Ciprofloxacin is a potent and widely used antibiotic that has been thoroughly researched and is now employed in current medicine [28–30]. Furthermore, with MICs ranging from 0.125 to 0.5 μg/mL, polyphemusin I is an antimicrobial peptide that demonstrates strong antimicrobial activity against Gram-negative and Gram-positive bacteria [31]. Therefore, ciprofloxacin and polyphemusin I were introduced as inhibitory groups. MIC values were determined as the lowest concentration by visually observing the degree of turbidity and measuring the absorbance OD_{600} in each well after incubation at 37 °C for 18 h, while the lowest concentration of bactericidal causing at least 99% killing of the initial inoculums was considered the minimum bactericidal concentration (MBC). MBC values were determined by extracting samples from wells with no apparent growth, followed by serial dilution and plating on LB agar plates for counting CFU. Every experiment was run three times.

2.7. Localization of FAM-labeled peptides in bacteria

To investigate the intracellular distribution of GAN-pep3 within

bacterial cells, we modified the N-terminus of GAN-pep3 with the fluorescent dye 5-carboxyfluorescein (5-FAM). The concentration of FAM-labeled GAN-pep3 was 1 × MIC for Gram-positive bacteria and 2 × MIC for Gram-negative bacteria, consistent with previous experimental conditions.

Bacterial cultures containing FAM-labeled GAN-pep3 and 0.1% PI (1 mg/mL) were incubated with shaking (150 rpm) at 37 °C. The concentration and incubation time of FAM-labeled GAN-pep3 were 1 × MIC for 10 min and 2 × MIC for 20 min for Gram-positive and Gram-negative bacteria, respectively. After incubation, the bacteria were centrifuged for 5 min at room temperature at 5000 ×g. The bacteria were rinsed twice with PBS buffer to remove the staining solution. The bacteria were subsequently fixed in 2.5% glutaraldehyde (GA) for 30 min in the dark. After fixation, the bacteria were centrifuged for 5 min at room temperature at 5000 ×g and resuspended in PBS buffer.

The bacterial cells were resuspended in 50 μL of PBS to prepare samples for microscopy. A mixture of 3.5 μL of this suspension and 1.5 μL of the mounting medium was applied onto the sliding glass and covered with a coverslip. The Leica TCS SP8 X Confocal Microscope (Leica Microsystems, Wetzlar, Germany) was used for confocal microscopic observation. Using a 488 nm laser as the excitation source, the emission for FAM was measured between 500 and 550 nm. The excitation and emission wavelengths for Propidium Iodide (PI) were 535 nm and 580–650 nm, respectively.

2.8. Scanning electron microscopy (SEM)

The bacteria culture that grew overnight was centrifuged for 7 min at 5500 rpm, and the pellets were then rinsed three times with 0.1 M PB. Bacteria were distributed in PB at a final concentration of 10^5 cfu/mL. Bacterial cultures containing GAN-pep3 at 1 × MIC were incubated with shaking (150 rpm) at 37 °C for 18 h. As control groups, bacterial cultures without GAN-pep3 were used. The bacteria were fixed overnight at 4 °C with 2.5% GA after being centrifuged for 10 min at 14000 ×g. The suspensions were resuspended in PB after centrifuging for 7 min at 14000 ×g three times. Pellets were dried using ethanol concentrations ranging from 30 to 100%. Subsequently, pellets were placed on a critical point dryer, and an ion sputter was used to cover the strains with gold. Samples were observed and imaged using a cold-filed emission scanning electron microscope (Hitachi S-4800).

2.9. Cryo soft X-ray tomography (Cryo-SXT)

Sample preparation before freezing followed a protocol like fluorescence microscopy experiments. *E. coli* was resuspended in PBS and diluted to 10^7 cfu/mL. Bacterial cultures containing FAM-labeled GAN-pep3 at 2 × MIC, 0.07% DAPI (1 mg/mL) and 0.1% PI (1 mg/mL) were incubated with shaking (150 rpm) at 37 °C for 20 min. Samples without FAM-labeled GAN-pep3 served as control groups. After incubation, the bacteria were centrifuged for 5 min at room temperature at 5000 ×g. The bacteria were rinsed twice with PBS buffer to remove the staining solution.

To prepare samples for pre-mapping and correlative imaging modalities [29], bacterial cells were resuspended in 50 μL of PBS. Then, an equal volume of gold nanoparticles (100 nm diameter, BBI Solutions, UK) was added for tilt series reconstruction [30]. Before the suspended samples were dropped onto the 3.05 mm gold grid (Quantifloil, Model: N1-C16nAuG1–01, Germany), the carbon side of the gold grid was treated with a glow discharger (PELCO easiGlowTM, USA) to increase hydrophilicity. A plunge freezer under liquid ethane was used to rapidly cool the gold grid containing the samples to temperatures below −170 °C. Fluorescence screening of the samples was then performed under cryo-correlative light with X-ray microscopy (CLXM) to facilitate subsequent soft X-ray tomography (SXT) image comparison. Data were collected from the beam line TPS 24A1 soft X-ray tomography endstation of NSRRC. The batch reconstruction procedures in IMOD aligned and rebuilt the tilt series [28].

2.10. Hemolysis assay

Fresh rat erythrocyte cells (RBCs) were collected in 3.2% sodium citrate vials, supported by Prof. Li-Jiuan Shen at the National Taiwan University Hospital. RBCs were centrifuged for 10 min at 3000 ×*g* at 4 °C. Following three times of PBS washing, RBCs were finally distributed in PBS at a final concentration of 8 × 10^9 cells/mL. Spectroscopic tests were used to measure the hemolytic activity. 180 μL of peptides with a diluted concentration mixed with 20 μL of RBCs into a 96-well microplate. The mixture was incubated for 30 min without shaking at 37 °C. Centrifuge the 96-well microplate at 300 ×*g* for 10 min by centrifuge (Eppendorf™, 5810R). 100 μL of supernatants were added to another 96-well microplate. The absorbance (λ = 540 nm) of samples with positive (distilled water) and negative (PBS) controls was measured with a microplate reader to determine the percentage of hemolysis [31]. Every experiment was run three times. Eq. (1) here we used to compute the percent of hemolysis.

$$\textit{Hemolysis rate}\ (\%) = \frac{OD_{test} - OD_{negative\ control}}{OD_{positive\ control} - OD_{negative\ control}} \times 100\% \quad (1)$$

2.11. Cell viability assay

Cells were plated in a 96-well microplate (5 × 103 cells/well) with 5 replicates per group for viability testing. Following a 24-h incubation period, peptides at various concentration (0–100 μM) were applied to cells for 48 h. Before using the microplate reader, the cells were treated with 10 μL of CCK-8 solution at 37 °C for an hour. In this investigation, there was a definite correlation between the absorbance at 450 nm and the number of cells. The half inhibitory concentration (IC50) value was computed using the percentage of inhibitory cells for peptides at different concentrations [32].

$$\textit{Cell viability}\ (\%) = \frac{OD_{treat} - OD_{blank}}{OD_{control} - OD_{blank}} \times 100\% \quad (2)$$

where ODtest, ODcontrol, and ODblank represent the absorbance of cells treated with both peptide and CCK-8, cells treated with CCK-8 alone, and CCK-8 solution without cells, respectively.

2.12. Statistical analysis

Descriptive statistics of the results, derived from at least three independent experiments, were presented as mean ± standard deviation (*SD*). One-way ANOVA was employed to compare the means between the groups, and Tukey's multiple comparisons test was then performed. The program GraphPad Prism 9.0 (GraphPad Software, San Diego, CA, USA) was used to conduct statistical analyses at a significance level of 0.05.

3. Results

3.1. Characterization of antimicrobial peptides

The physicochemical properties of the designed peptides were determined by BACHEM and Peptide 2.0 Inc. (Table 1). All peptides range in length from 13 to 30 amino acids. The molecular weights range from 1440.64 to 3868.29 g/mol. Most of these peptides are positively charged from +1.0 to +9.8 eV under neutral conditions, whereas Pep-1v (−4.2 eV) and Pep-7c (−1.0 eV) are negatively charged. The hydrophobicity of peptides in this study ranges from 16.67% to 62.50%. However, peptides such as Pep-1v, Pep-3 m, and AFP_23_gag_18, with respective hydrophobicities of 20.00%, 30.00%, and 16.67%.

Table 1
Physicochemical properties of peptides.

Peptide	Length	Molecular weight (g/mol)	Net charge (eV) at pH 7.4 [a]	Hydrophobicity (%) [b]
GAN-pep1	19	1941.31	+1.9	52.63
GAN-pep2	27	3074.79	+5.4	48.51
GAN-pep3	26	2906.54	+5.8	53.85
GAN-pep4	26	2886.55	+5.8	50.00
GAN-pep5	29	3034.61	+3.9	55.17
GAN-pep6	22	2498.12	+4.5	59.06
GAN-pep7	25	2623.16	+2.7	44.00
GAN-pep8	21	2430.98	+4.9	47.62
Pep-1v	30	3868.29	−4.2	20.00
Pep-3 m	20	2552.21	+9.8	30.00
Pep-6f	13	2000.47	+6.9	46.15
Pep-7c	13	1440.64	−1.0	46.15
Pep-8 m	24	2782.56	+9.8	58.33
Pep-9m_g	26	2977.59	+5.0	42.31
ACP_23_gag_24	24	2595.26	+3.1	62.50
AMP_23_gag_20	20	2371.94	+5.9	45.00
AFP_23_gag_18	18	2227.84	+4.5	16.67
AVP_23_gag1_23	23	2453.83	+1.0	43.38

[a] BACHEM (https://www.bachem.com/) computed the net charge at pH 7.4.
[b] Hydrophobicity (%) is the relative abundance of hydrophobic amino acids in a peptide estimated by Peptide 2.0 Inc. (https://www.peptide2.com/).

3.2. Secondary structure analysis of peptides by circular dichroism (CD)

Circular dichroism (CD) spectroscopy evaluated each peptide's secondary structure in different environments. As shown in Fig. 2, the CD spectra of peptides prepared in 10 mM PB revealed a big negative peak at 200 nm, indicating the random coil conformation. In contrast, all the peptides except for Pep-6f and AFP_23_gag_18 altered their secondary structures when mixed with SDS micelles, which can operate as a model for the surface of bacteria [33,34]. These peptides displayed typical α-helical conformations with a significantly increased fractional helicity. TEF buffer could induce peptides to form α-helical conformation at low concentrations and reach the highest fractional helicity at 50% TFE [35,36]. However, the fractional helicity shown in TFE represents the relative propensity of the peptides to adopt an α-helical conformation rather than the actual secondary structure of the peptides [37]. When mixed with 50% TFE buffer, most of the peptides also changed their structures into α-helical conformations. However, Pep-6f and AFP_23_gag_18 favored forming β-sheet structures such as parallel or anti-parallel configurations rather than α-helical conformation. Gram-negative bacteria have a significant amount of LPS in their outer membranes. It is the initial contact site for peptides when interacting with bacteria [38,39]. Most peptides showed distinctive peaks from the α-helical conformation. Nevertheless, compared to 50% TFE, various peptides such as GAN-pep3, GAN-pep5, GAN-pep6, GAN-pep7, GAN-pep8, Pep-3 m, Pep-6f, Pep-7c, Pep-8 m, and Pep-9m_g presented a higher percentage of anti-parallel structure in LPS micelles.

3.3. Zone of inhibition

The disk diffusion experiment was first used to evaluate the antibacterial activity of peptides. Ciprofloxacin, a broad-spectrum antibiotic targeting DNA gyrase [40], and polyphemusin I, a cationic peptide from horseshoe crab [41], were the controls. The inhibition zone with the mean value ± standard deviation of each peptide and ciprofloxacin is shown in Fig. 3. A one-way ANOVA revealed a significant difference in inhibition zone among the different peptide treatments ($F(19, 40) = 1860$, $p < 0.01$). Post-hoc Tukey's HSD tests indicated that groups marked with letters differed significantly ($p < 0.05$). The results depicted in Table 2 reveal that ciprofloxacin-loaded cotton fibers exhibited the largest inhibition zone of 2.97 ± 0.05 cm against *E. coli* compared with all other treatments ($p < 0.05$). In the case of polyphemusin I, it showed strong antimicrobial activity against *E. coli*, while other peptides, including GAN-pep2, GAN-pep3, GAN-pep4, and Pep-9m_g, also showed a similar effect, with inhibition zones ranging from 1.45 to 1.54 cm. Among the peptides we designed, GAN-pep2, GAN-pep3, GAN-pep4, GAN-pep8, Pep-8 m, and Pep-9m_g caused similar inhibition zone sizes, ranging from 1.40 to 1.51 cm. The inhibition zones for other peptides, including GAN-pep5, Pep-3 m, Pep-6f, and AMP_23_gag_20, were smaller, measuring 1.29 to 1.34 cm. Conversely, other peptides exhibited less evident inhibition zones, including GAN-pep1, GAN-pep6, GAN-pep7, Pep-1v, Pep-7c, ACP_23_gag_24, AFP_23_gag_18, and AVP_23_gag1_23 (the results were provided in **S2**).

Table 2
Inhibition zone of AMPs and ciprofloxacin at 500 μg/mL against *E. coli* (1.0×10^8 cfu/mL) after 18 h.

AMPs	Inhibition zone (cm)	AMPs	Inhibition zone (cm)
GAN-pep1	0.07 ± 0.01	Pep-6f	1.29 ± 0.03
GAN-pep2	1.47 ± 0.01	Pep-7c	0.06 ± 0.00
GAN-pep3	1.45 ± 0.06	Pep-8 m	1.40 ± 0.03
GAN-pep4	1.48 ± 0.04	Pep-9m_g	1.51 ± 0.06
GAN-pep5	1.30 ± 0.04	ACP_23_gag_24	0.08 ± 0.01
GAN-pep6	0.06 ± 0.00	AMP_23_gag_20	1.34 ± 0.03
GAN-pep7	0.06 ± 0.00	AFP_23_gag_18	0.09 ± 0.01
GAN-pep8	1.43 ± 0.02	AVP_23_gag1_23	0.08 ± 0.01
Pep-1v	0.10 ± 0.00	Polyphemusin I	1.54 ± 0.01
Pep-3 m	1.31 ± 0.07	Ciprofloxacin	2.97 ± 0.05

3.4. Minimum inhibitory concentration (MIC) and minimum bactericidal concentration (MBC)

The MIC and MBC values of AMPs and ciprofloxacin are shown in Table 3 and Table 4. Most of the designed peptides showed antimicrobial activity against *E. coli,* with MICs ranging from 0.42 to 26.1 μM. Polyphemusin I demonstrated remarkable antimicrobial activity against *E. coli*, with a MIC of 0.29 μM. Notably, the antimicrobial activities of GAN-pep2, 3, 4, and AMP_23_gag_20 were comparable to that of polyphemusin I. Some peptides, including GAN-pep3, Pep-9m_g, and ACP_23_gag_24, exhibited broad-spectrum antimicrobial activity. These peptides had MICs ranging from 1.03 to 15.1 μM against both tested Gram-negative bacterium carbapenem-susceptible and carbapenem-resistant *P. aeruginosa*. Furthermore, their MIC values were between 1.54 and 3.56 μM for the methicillin-susceptible strain of *S. aureus* and 3.08 and 15.1 μM for the methicillin-resistant strain. Notably, the MBC of GAN-pep3 was >3 times the MIC against Gram-positive bacteria but only 1 to 2 times the MIC against Gram-negative bacteria. For Pep-9m_g, only the MBC of *E. coli* was 2 times its MIC; all other values were identical. ACP_23_gag_24 had an MBC value of 2 times or higher than its MIC for all bacteria.

3.5. GAN-pep3 localization within bacterial cell membranes

Peptide localization experiments were conducted using confocal microscopy to observe FAM-labeled GAN-pep3. All images were acquired using a × 100 oil immersion lens. For clarity, a representative region of each image was selected and magnified digitally at ×5. The fluorescence of FAM-labeled GAN-pep3 and PI overlapped in *E. coli*, indicating that GAN-pep3 translocated into the cell (Fig. 4). Additionally, the stronger green fluorescence on the *E. coli* bacterial membrane suggested that GAN-pep3 localized primarily on the bacterial membrane (Fig. 5A). Similarly, FAM-GAN-pep3 predominantly accumulated on the bacterial membranes of *P. aeruginosa* and CRPA. In the merged images, the red fluorescence of PI was present within the bacteria and at the sites of bacterial fragments (Fig. 5B and C), indicating severe membrane damage caused by GAN-pep3, with no green fluorescence from the peptide detected. For *S. aureus* and MRSA, FAM-GAN-pep3 accumulated on the bacterial membrane and exhibited yellow fluorescence in the

Table 3
Antimicrobial activity (MIC, μg/mL or μM) of designed peptides, polyphemusin I, and ciprofloxacin against five tested bacterial strains.

Bacteria Species	Gram-negative			Gram-positive	
	E. coli	*P. aeruginosa*		*S. aureus*	
Strain	SG12009	CSPA[a] S07-10-0059	CRPA[b] M06-06-0213	MSSA[c] S01-10-0202	MRSA[d] N07-10-0043
GAN-pep1	NA [e]	NA	NA	NA	NA
GAN-pep2	2 / 0.62	50 / 16.3	5 / 1.63	NA	NA
GAN-pep3	2 / 0.69	3 / 1.03	3 / 1.03	5 / 1.72	30 / 10.3
GAN-pep4	2 / 0.69	50 / 17.3	3 / 1.03	NA	NA
GAN-pep5	22.5 / 7.41	NA	NA	NA	NA
GAN-pep6	NA	NA	NA	NA	NA
GAN-pep7	NA	NA	NA	NA	NA
GAN-pep8	50 / 20.6	NA	NA	10 / 4.11	45 / 18.5
Pep-1v	NA	NA	NA	NA	NA
Pep-3 m	8 / 3.13	NA	10 / 3.91	NA	NA
Pep-6f	45 / 22.5	NA	NA	NA	NA
Pep-7c	NA	NA	NA	NA	NA
Pep-8 m	25 / 8.98	NA	NA	NA	NA
Pep-9m_g	6 / 2.02	45 /15.1	45 / 15.1	10 / 3.56	45 / 15.1
ACP_23_gag_24	16 / 6.17	32 / 12.3	32 / 12.3	4 / 1.54	8 / 3.08
AMP_23_gag_20	2 / 0.42	32 / 13.5	32 / 13.5	NA	NA
AFP_23_gag_18	NA	NA	NA	NA	NA
AVP_23_gag1_23	64 / 26.1	32 / 13.0	32 / 13.0	32 / 13.0	64 / 26.1
Polyphemusin I	0.7 / 0.29	NA	NA	NA	NA
Ciprofloxacin	0.031/ 0.097	0.13/ 0.38	8 / 24	0.25/ 0.75	0.25/ 0.75

[a] *P. aeruginosa* S07-10-0059 is a carbapenem-susceptible strain which is known as *CSPA*.
[b] *P. aeruginosa* N06-06-0213 is a carbapenem-resistant strain which is known as *CRPA*.
[c] *S. aureus* S01-10-0202 is a methicillin-susceptible strain which is known as *MSSA*.
[d] *S. aureus* N07-10-0043 is a methicillin-resistant strain which is known as *MRSA*.
[e] NA: the peptide was shown to be ineffective against the bacteria when they kept growing at the highest concentration (64 μg/mL) that was applied.

Table 4
The minimal bactericidal concentration (MBC, μg/mL or μM) of designed peptides and ciprofloxacin against five tested bacterial strains.

Bacteria Species	Gram-negative			Gram-positive	
	E. coli	*P. aeruginosa*		*S. aureus*	
Strain	SG12009	CSPA S07-10-0059	CRPA M06-06-0213	MSSA S01-10-0202	MRSA N07-10-0043
GAN-pep1	NA [a]	NA	NA	NA	NA
GAN-pep2	3.12 / 1.01	50 / 16.3	10 / 3.25	NA	NA
GAN-pep3	4 / 1.38	3 / 1.03	3 / 1.03	>15/ >5.16	>60/ >20.6
GAN-pep4	4 / 1.39	50 / 17.3	9 / 3.12	NA	NA
GAN-pep5	>64/ >21.1	NA	NA	NA	NA
GAN-pep6	NA	NA	NA	NA	NA
GAN-pep7	NA	NA	NA	NA	NA
GAN-pep8	>64/ >26.3	NA	NA	>30/ >12.3	>45/ >18.5
Pep-1v	NA	NA	NA	NA	NA
Pep-3 m	24 / 9.40	NA	20 / 7.84	NA	NA
Pep-6f	>64/ >32.0	NA	NA	NA	NA
Pep-7c	NA	NA	NA	NA	NA
Pep-8 m	>64/ >23.0	NA	NA	NA	NA
Pep-9m_g	12 / 4.03	45 /15.1	45 / 15.1	10 / 3.56	45 / 15.1
ACP_23_gag_24	32 / 12.3	64 / 24.6	>64/ >24.6	>12/ >4.62	>24/ >9.25
AMP_23_gag_20	4 / 1.69	>64/ >27.0	64 / 27.0	NA	NA
AFP_23_gag_18	NA	NA	NA	NA	NA
AVP_23_gag1_23	64 / 26.1	64 / 26.1	32 / 13.0	>64/ >26.1	>64/ >26.1
Ciprofloxacin	0.063/ 0.19	0.25/ 0.75	32 / 96	0.25/ 0.75	0.5 / 1.5

[a] NA: the peptide was shown to be ineffective against the bacteria when they kept growing at the highest concentration (64 μg/mL) that was applied.

merged images, suggesting that GAN-pep3 may penetrate the bacterial and enter the interior (Fig. 5D and E). Furthermore, the red fluorescence of PI surrounding the bacteria indicated the absence of an intact bacterial membrane, with internal substances exposed.

3.6. SEM visualization of GAN-pep3-induced bacterial membrane disruption

We investigated the morphological effects of GAN-pep3 at 1 × MIC on *E. coli*, *P. aeruginosa*, CRPA, *S. aureus*, and MRSA. The findings demonstrated that the membrane shape of treated and untreated bacteria differed significantly (Fig. 6). Bacterial membranes without treatment were smooth, turgid, and undamaged (Fig. 6A, C, E, G, and I). In contrast, the addition of GAN-pep3 significantly altered the cellular morphology of *E. coli*, causing flaky membrane pieces, surface wrinkles, and holes (Fig. 6B). Similarly, GAN-pep3 treatment caused wrinkled membranes and cell debris in *P. aeruginosa* and CRPA (Fig. 6D and F). For *S. aureus*, GAN-pep3 treatment led to minor blebbing on the surface (Fig. 6H). The damage was even more pronounced in MRSA, where the original form was unrecognizable (Fig. 6J).

3.7. Bacterial membrane visualized by soft x-ray tomography (SXT)

E. coli was selected as a model organism to investigate the membrane-disrupting effects of GAN-pep3. Reconstructed slices from Cryo-Soft X-ray Tomography (Cryo-SXT) are shown in Fig. 7. In the untreated group, bacterial membranes appeared smooth and intact, with clearly defined nucleoids observed as lighter zones within the denser cytoplasm (Fig. 7A, blue arrows). In contrast, cells treated with GAN-pep3 exhibited clear signs of membrane damage, including discontinuities and faults along the membrane surface (Fig. 7B, red arrows). These defects were accompanied by the appearance of transparent regions, indicating cytoplasmic loss [42]. Additionally, the internal contrast of treated bacteria was greatly reduced, resembling that of the carbon film, suggesting leakage of intracellular contents (Fig. 7C, red arrow).

Consistent with these observations, GAN-pep3 was shown to cause holes and surface depressions in the bacterial membrane, as evidenced by alterations in membrane structure and surface morphology seen in Figs. 7 and 8. Interestingly, Fig. 7B and C, captured during the same experiment, displayed different stages or outcomes of peptide-induced damage. We hypothesize that GAN-pep3 induces pore formation in the *E. coli* membrane, leading to cytoplasmic leakage at varying degrees. In some cells, membrane permeability increased, resulting in partial content loss (Fig. 7B), while in others, nearly complete leakage occurred, leaving only the bacterial outline visible (Fig. 7C). These findings support the membrane-disruptive mechanism of GAN-pep3 as a key contributor to its antibacterial activity.

The continuous slices of treated *E. coli* are shown in Fig. 8. The top slice showed a disruption in the membrane border of *E. coli* and a decrease in internal contrast, suggesting internal materials were leaking (Fig. 8A, red arrow). The membrane rupture hole grew wider as the slice descended, and an interior cavity was visibly created. This suggests that GAN-pep3 may concentrate here, damaging the bacterial membrane and further leakage of internal substances (Fig. 8B, C, and D, red arrow). These results demonstrate that GAN-pep3 can directly harm the bacterial membrane and cause the leakage of internal substances.

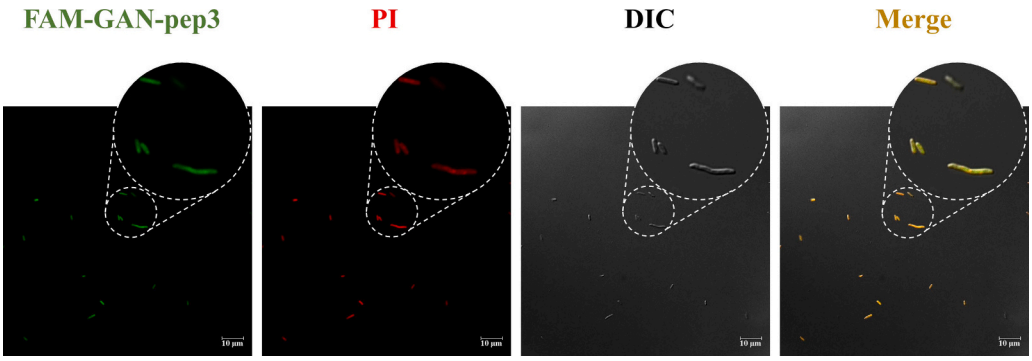

Fig. 4. Translocation of FAM-GAN-pep3. Fluorescence confocal microscopy images depict *E. coli* treated with FAM-labeled GAN-pep3 at 2 × MIC and stained with PI dye. Green fluorescence indicates the localization of the peptide within the cells. Red fluorescence shows the nucleic acids stained by PI. Scale bar: 10 μm. (For interpretation of the references to colour in this figure legend, the reader is referred to the web version of this article.)

3.8. Safety and therapeutic index of peptides

Erythrocytic cells incubated with various peptide concentrations were used to determine the lysis rate and assess the peptides' hemolytic activity (Fig. 9). Most AMPs exhibited a dose-dependent response, with an increased hemolysis rate corresponding to higher peptide concentrations. Pep-3 m, Pep-6f, Pep-7c, AMP_23_gag_20, and AFP_23_gag_18 showed minimal hemolytic activity among the tested peptides. Conversely, other AMPs exhibited hemolytic activity. The values of MHC_{10} from the highest to the lowest were AVP_23_gag1_23 (36.9 μM), ACP_23_gag_24 (16.8 μM), GAN-pep3 (13.9 μM), Pep-8 m (10.5 μM), and Pep-9m_g (3.95 μM) (Table 5). It is noteworthy that four AMPs, including ACP_23_gag_24, AMP_23_gag_20, AFP_23_gag_18, and AVP_23_gag1_23, were designed to have low hemolytic activity from AI models and indeed exhibited reduced hemolysis compared to other AMPs.

The selectivity of antimicrobial drugs for bacteria instead of erythrocytes is used to assess their therapeutic potential [12]. The therapeutic index (TI) measures peptide selectivity by taking the geometric mean (GM) of MIC values against tested bacteria and the concentration of peptide leading to 10% fresh red blood to lyse [43,44]. Among all tested peptides, AMP_23_gag_20 and Pep-3 m demonstrated the highest TI value against Gram-negative bacteria, with TI (−) values of 30.1 and 23.5, respectively, attributed to their low hemolysis rates. Although GAN-pep3 had broad-spectrum antimicrobial activity, it exhibited some hemolytic activity; however, its GM was the lowest among all peptides against Gram-negative bacteria, resulting in a TI (−) value of 15. Furthermore, ACP_23_gag_24 showed the highest TI (+) value against Gram-positive bacteria at 7.71, due to the lowest GM (+) value.

3.9. The cytotoxicity to human normal cells

The cytotoxicity of AMPs was tested in human pulmonary fibroblast HPF-a cells. Most AMPs were cytotoxic to HPF-a cells (Fig. 10). Table 6 displays the AMP concentrations required to decrease HPF-a cell viability by 50% (IC_{50}), which were determined. The most cytotoxic substances against HPF-a cells were Pep-8 m and GAN-pep8, which had IC_{50} values of 3.99 and 4.54 μM, respectively. The IC_{50} values for GAN-pep3 and Pep-9m_g was 9.96 and 9.32 μM, respectively, indicating moderate cytotoxicity. However, at the highest concentrations of Pep-3 m and Pep-6f, cell viability was significantly reduced. Finally, at all investigated concentrations, Pep-7c exhibited negligible cytotoxicity and no discernible cell mortality.

4. Discussion

Leveraging the powerful capabilities of Generative Adversarial Networks (GANs), the rapid development of highly effective and low-toxic antimicrobial peptides (AMPs) has become an achievable goal. AMPs possess a unique antibacterial mechanism: they form a specific secondary structure on the bacterial outer membrane, subsequently leading to bacterial membrane perforation and reduced stability, thereby superseding traditional antibiotics [45]. In this study, we selected the WGAN-GP model primarily due to its exceptional training stability and notable ability to mitigate mode collapse, a significant hindrance to diversity in generative models. With WGAN-GP, we successfully generated diverse peptide candidates that retained AMP-like physicochemical characteristics. While we compared WGAN-GP with the original GAN model in our previous work, we acknowledge that we have not yet benchmarked our approach against newer generative models such as Diffusion Models or Variational Autoencoders (VAEs). This remains a limitation, and we plan to address these more extensive comparisons in our next publications.

This study proposes an innovative approach to AMP discovery and design, utilizing AI-guided methodologies to enhance antimicrobial activity. We selected top-ranked 18 AMP candidates (GAN-pep1–8, Pep-1v – Pep-9m_g, and ACP_23_gag_24 – AVP_23_gag1_23) to evaluate their antimicrobial efficacy.

Disk diffusion testing revealed that 10 candidates exhibited antimicrobial activity against *E. coli*. GAN-pep3, Pep-9m_g, and ACP_23_gag_24 were identified as having broad-spectrum antimicrobial effects, showing their effectiveness in suppressing antibiotic-resistant bacteria growth used in MIC assay. Notably, GAN-pep3 demonstrated remarkable and rapid broad-spectrum antimicrobial activity, comparable to antibiotics like vancomycin and ciprofloxacin [46,47]. However, it is worth noting that the MIC of GAN-pep3 against Gram-negative bacteria is lower than that against Gram-positive bacteria. This variation could be attributed to the structural differences between Gram-negative and Gram-positive bacteria.

Studies have shown that AMPs with net charges ranging from +3 to +8 enhance antimicrobial activity [48,49]. Our findings align with this observation, showing that GAN-pep3, Pep-9m_g, and ACP_23_gag_24, with net charges of +5.8, +5.0, and + 3.1, respectively, exhibit broad-spectrum antimicrobial activity. However, excessive charge can reduce peptide efficacy by causing repulsion between adjacent peptides [50]. Pep-3 m and Pep-8 m, with net charges of +9.8, exhibit low antimicrobial activity against *E. coli*. Their MIC values are 4.5 times (3.13 μM) and 13 times (8.98 μM) that of GAN-pep3 (MIC = 0.69 μM), respectively.

Furthermore, the secondary structures of peptides affect their antimicrobial activity. Peptides can interact with and disrupt microbial cell membranes because of their amphipathic α-helical structures [51]. According to our findings, the broad-spectrum antimicrobial properties of GAN-pep3, Pep-9m_g, and ACP_23_gag_24 have α-helical proportions ranging from 21.1 to 51.3%. Nevertheless, the α-helical proportions of GAN-pep6, GAN-pep7, Pep-1v, and Pep-7c, which exhibited no antimicrobial activity, ranged from 0.00 to 8.80%. GAN-pep1 and

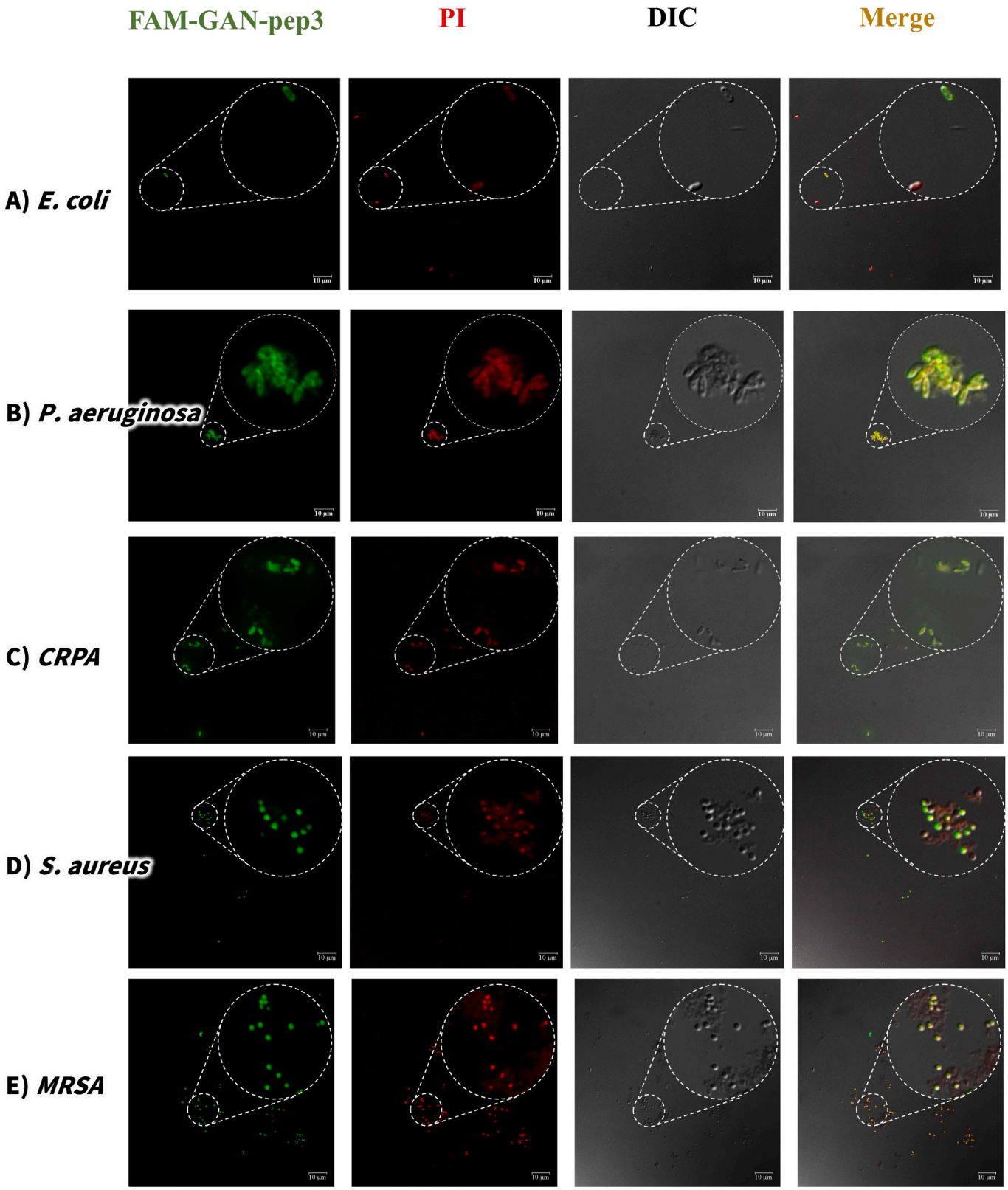

Fig. 5. Localization of FAM-GAN-pep3 within bacterial cells. Fluorescence confocal microscopy images depict (A) *E. coli*, (B) *P. aeruginosa*, and (C) CRPA treated with FAM-labeled GAN-pep3 at 2 × MIC, and (D) *S. aureus* and (E) MRSA treated with FAM-labeled GAN-pep3 at 1 × MIC. All bacterial cells were stained with PI dye. Green fluorescence indicates the localization of the peptide within the cells. Red fluorescence shows the nucleic acids stained by PI. Scale bar: 10 μm. (For interpretation of the references to colour in this figure legend, the reader is referred to the web version of this article.)

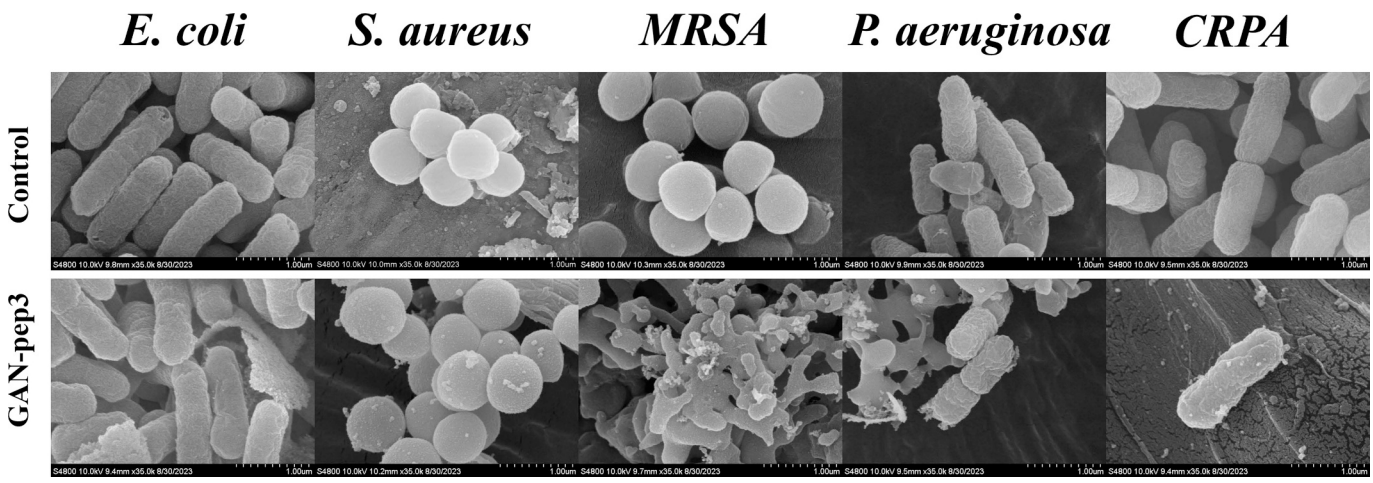

Fig. 6. HRSEM images of bacteria. (A), (B) *E. coli*, (C), (D) *P. aeruginosa*, (E), (F) CRPA, (G), (H) *S. aureus*, and (I), (J) MRSA treated with or without GAN-pep3 at 1 × MIC.

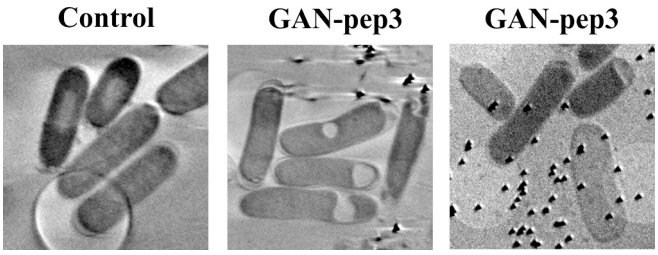

Fig. 7. Tomographic reconstructed slices of *E. coli* (A) without treatment and (B) (C) treated with GAN-pep3. The blue triangles indicate the nucleoids inside the bacteria, and the red ones indicate the membrane damage caused by designed peptides. (For interpretation of the references to colour in this figure legend, the reader is referred to the web version of this article.)

AFP_23_gag_18 did not show any antimicrobial properties despite having α-helical proportions of 25.9% and 22.0%, respectively. GAN-pep1 had an inadequate charge (+1.9 eV), and AFP_23_gag_18 had insufficient hydrophobicity (16.67%), which prevented them from interacting with the bacterial cell membrane surface.

We speculate that GAN-pep3 uses a carpet-like mechanism to promote membrane permeabilization and destruction. According to the mechanism analysis, GAN-pep3 exhibits a random coil configuration in an aqueous solution environment. Once it contacts the bacterial surface, it transforms into an α-helical structure and attaches to the bacterial cell membrane. Six consecutive hydrophobic amino acids (Ala^{20}, Leu^{21}, Pro^{22}, Ala^{23}, Ile^{24}, and Ile^{25}) at its C-terminal can partially penetrate the bilayer hydrocarbon core and promote membrane permeabilization. GAN-pep3 damaged the bacterial cell membrane, causing holes and depressions on the bacterial surface, as validated by observations of alterations on the bacterial surface and cell membrane. X-ray tomography revealed a discontinuous cell membrane surface (Fig. 7B and 8). Furthermore, it was discovered that Fig. 7B and C exhibited distinct results within the identical experimental process. We hypothesized that GAN-pep3 caused a hole in the *E. coli* cell membrane, allowing some cytoplasm to leak (Fig. 7B, red arrow). The bacteria, on the other hand, merely left a more noticeable outline. This could be due to GAN-pep3 making the cell membrane more permeable, allowing more cytoplasm to escape (Fig. 7C, indicated by the red arrow).

Finally, the biological activity of synthetic AMPs used in medicine should be assessed. The biosafety of these peptides was evaluated using hemolysis assays. The results showed that AMP_23_gag_20 (TI = 30.1), Pep-3 m (TI = 23.5), and GAN-pep3 (TI = 15.4) exhibited great therapeutic index values against Gram-negative bacteria, and ACP_23_gag_24 (TI = 7.71) exhibited the greatest value against Gram-positive bacteria. These peptides demonstrated higher therapeutic potential than Melittin (TI = 0.18) [31], Cecropin A (TI = 21.3) [52], and HEA-9 (TI = 6.32) [53].

On the other hand, HPF-a cells were used to conduct the peptide's cytotoxicity assay. The findings demonstrated the considerable cytotoxicity of several AMPs to HPF-a, including GAN-pep8 and Pep-8 m. The interactions between peptides and healthy cell membranes are mostly driven by hydrophobic interactions [54]. Consequently, one of the potential causes of the harmful effects of Pep-8 m on healthy cells is its high hydrophobicity (58.33%). Furthermore, the peptide orientation affects the interaction between peptides and cell membranes [55]. The survival of HPF-a cells was somewhat affected by the helical GAN-pep3, GAN-pep8, Pep-8 m, and Pep-9m_g. In contrast, HPF-a cells were barely affected by Pep-6f and Pep-7c.

This study highlights the strengths of the WGAN-GP architecture in generating AMP candidates that closely mimic natural AMPs in sequence and function, with high success rates in vitro. Its stability and resistance to mode collapse allow for reliable exploration of novel sequence space. Still, the lack of structure-based learning and the need to benchmark against other generative models remain limitations. The identified peptides, particularly GAN-pep3, show promising therapeutic potential, outperforming known AMPs in both potency and selectivity. These candidates could be applied in clinical settings, such as topical antimicrobials or catheter coatings. However, commercialization will require overcoming key challenges, including synthesis cost, in vivo stability, and delivery. Future work will focus on refining the model through structure-aware training, conducting in vivo studies aligned with the 3R principles, and integrating high-throughput screening pipelines. These efforts aim to bridge the gap between in silico peptide generation and clinical application.

5. Conclusions

We successfully designed novel antimicrobial peptides (AMPs) to investigate their antimicrobial properties and biosafety features. The intended AMPs ranged in charge from −1.0 to +9.8, their hydrophobicity from 16.67% to 59.06%, and their length ranged from 13 to 30 amino acids. Given that the secondary structure of antimicrobial peptides (AMPs) plays a crucial role in their antimicrobial properties, our findings indicate that most AMPs in this study exhibit a helical structure in a bacterial membrane-like environment. According to the data, the results showed that the designed peptides exhibited desirable antimicrobial activity, which was significantly better than that of antibiotics. GAN-pep3-induced damage and increased membrane permeabilization

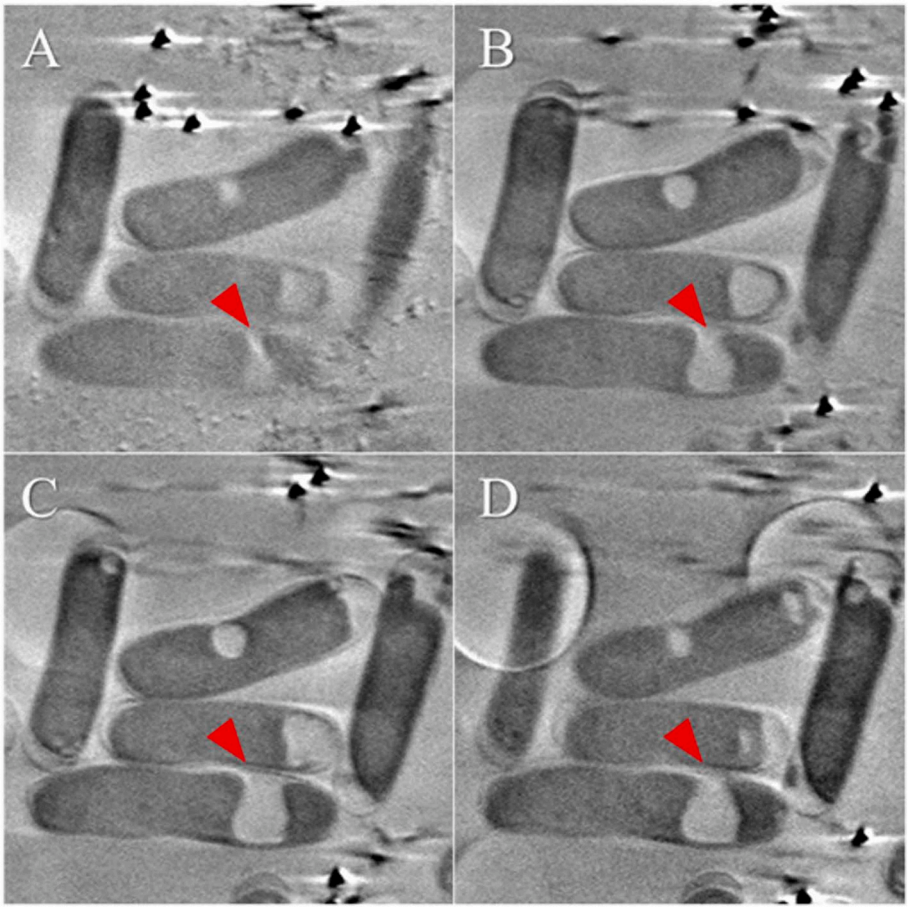

Fig. 8. Tomographic reconstruction of different slices of *E. coli* treated with GAN-pep3. The vertical slices are (A) to (D) from top to bottom. The red triangles indicate the membrane damage caused by designed peptides. (For interpretation of the references to colour in this figure legend, the reader is referred to the web version of this article.)

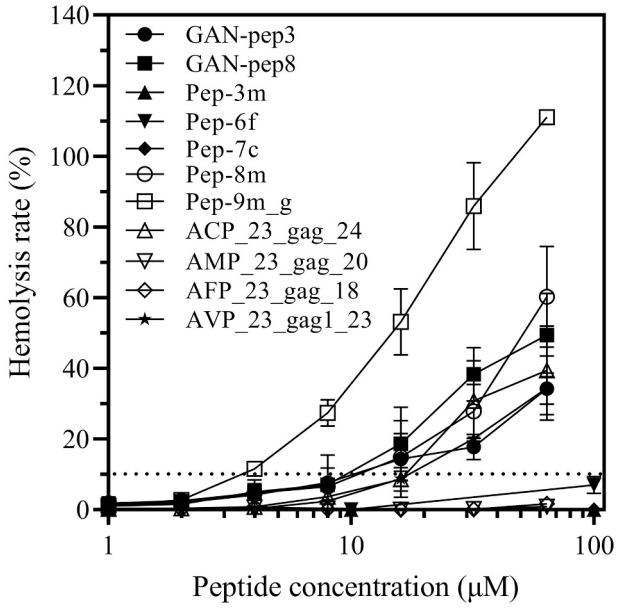

Fig. 9. The hemolytic activity of peptides. Error bars represent the ± standard deviations of three repeated measurements.

Table 5
Geometric mean (GM) of MIC for Gram-negative (−) and positive bacteria (+), minimal hemolytic concentration (MHC), and therapeutic index (TI)[a] for the analyzed AMPs.

AMPs	GM (−)	GM (+)	MHC_{10}[b] (μM)	TI (−)	TI (+)
GAN-pep3	0.90	4.21	13.9	15.4	3.30
GAN-pep8	38.5	8.72	8.36	0.217	0.959
Pep-3 m	8.50	50.2	> 100	23.5	3.98
Pep-6f	45.2	64.0	> 100	4.43	3.13
Pep-7c	88.8	88.8	> 100	2.25	2.25
Pep-8 m	26.7	46.0	10.5	0.393	0.23
Pep-9m_g	7.72	7.33	3.95	0.51	0.54
ACP_23_gag_24	9.77	2.18	16.8	1.72	7.71
AMP_23_gag_20	4.25	54.0	> 64	30.1	2.37
AFP_23_gag_18	57.4	57.4	> 64	2.23	2.23
AVP_23_gag1_23	16.4	18.4	36.9	2.25	2.00

[a] TI was calculated as MHC_{10}/GM.
[b] 10% of minimal hemolysis concentration (MHC_{10}) was characterized as the lowest concentration inducing 10% hemolysis.

were observed due to its broad-spectrum antimicrobial activity. The carpet-like mechanism of destroying bacterial membranes was linked to this peptide's antimicrobial effect. Additionally, GAN-pep3 offered benefits for medicinal applications and was more selective for bacteria than red blood cells.

Although it appears promising, further research and refinement are necessary before AI-designed AMPs can be effectively utilized in clinical settings. Future clinical trials are necessary to evaluate the safety and effectiveness of these approaches in human participants, as in vivo

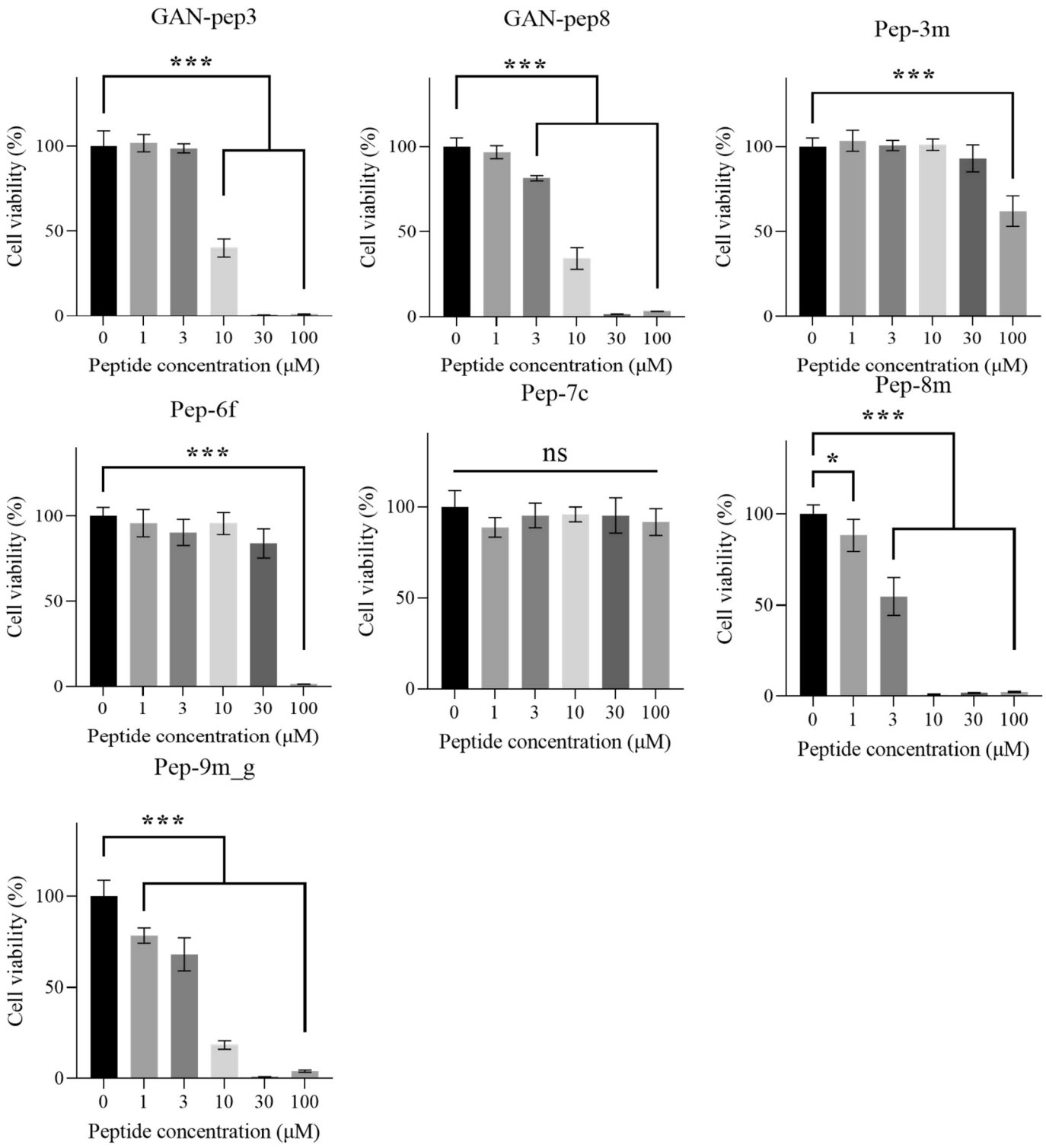

Fig. 10. Cell viability rate of HPF-a after treated with GAN-pep3, GAN-pep8, Pep-3 m, Pep-6f, Pep-7c, Pep-8 m, and Pep-9m_g for 48 h. Data is expressed as the mean ± *SD*. * $p < 0.05$, ** $p < 0.01$ and *** $p < 0.001$ vs. 0 μM group.

studies employing animal models have yielded valuable insights. Their potential as useful additions to the toolkit of contemporary medicine in the fight against infectious diseases will be ascertained through further research and clinical studies.

CRediT authorship contribution statement

Chia-Wen Lai: Writing – original draft, Validation, Methodology, Formal analysis, Data curation, Conceptualization. **Chung-Yen Lin:** Writing – review & editing, Writing – original draft, Project administration, Investigation, Funding acquisition, Conceptualization. **Meng-Chen Tsai:** Validation, Methodology, Formal analysis. **Wei-Jung Chen:** Methodology. **Chia-Chun Hsieh:** Methodology, Validation. **Zi-Jing Lin:** Validation. **Li-Jiuan Shen:** Resources, Methodology. **Ying-Lien Chen:** Resources, Methodology. **Lee-Jene Lai:** Software, Resources, Methodology. **Shu-Hwa Chen:** Writing – original draft, Supervision, Resources,

Table 6
Cytotoxicity (IC_{50}, μM) of peptides against HPF-a cells at 48 h.

Peptides	HPF-a
GAN-pep3	9.96
GAN-pep8	4.54
Pep-3 m	>100
Pep-6f	51.9
Pep-7c	–
Pep-8 m	3.99
Pep-9m_g	9.32

Project administration, Investigation, Funding acquisition, Conceptualization. **Yang-Hsin Shih:** Writing – review & editing, Supervision, Project administration, Investigation, Funding acquisition, Conceptualization.

Declaration of competing interest

The authors declare the following financial interests/personal relationships which may be considered as potential competing interests:

Yang-Shin Shih, Shu-Hwa Chen reports financial support was provided by the National Science and Technology Council and the Ministry of Education. If there are other authors, they declare that they have no known competing financial interests or personal relationships that could have appeared to influence the work reported in this paper.

Acknowledgments

The authors thank the fund 112-2221-E-001 -018 -MY3 and NSTC 113-2314-B-001-013 to C. Y. Lin, NSTC 113-2221-E-038 -020 -MY3 and the grant from The Featured Areas Research Center Program within the framework of the Higher Education Sprout Project by the Ministry of Education (MOE) to S. H. Chen and 106-2221-E-002-043-MY3 to Y. S. Shih by the National Science and Technology Council (NSTC), Taiwan, and partly sponsored by the grant (NTUAS-111L04312) from National Taiwan University and Academia Sinica, Taiwan, for financially supporting this research and publication.

Data availability

The dataset and source code for AMP-GAN are available on GitHub at https://github.com/lsbnb/amp_gan.

References

[1] N. SF, U.F. Gohar, S.F. Tahir, H. Mukhtar, S. Pornpukdeewattana, P. Nukthamna, A.M. Moula Ali, S.C.B. Bavisetty, S. Massa, Antimicrobial resistance: more than 70 years of war between humans and bacteria, Crit. Rev. Microbiol. 46 (5) (2020) 578–599.
[2] H. Madni, H.A. Mohamed, H.A.M. Abdelrahman, C.A. dos Santos-Silva, A. M. Benko-Iseppon, Z. Khatir, N.O. Eltai, N.A. Mohamed, S. Crovella, In silico-designed antimicrobial peptide targeting MRSA and Ecoli with antibacterial and antibiofilm actions, Sci. Rep. 14 (1) (2024) 12127.
[3] A.M. Almansour, M.A. Alhadlaq, K.O. Alzahrani, L.E. Mukhtar, A.L. Alharbi, S. M. Alajel, The silent threat: antimicrobial-resistant pathogens in food-producing animals and their impact on public health, Microorganisms 11 (9) (2023) 2127.
[4] R. Xiao, D. Huang, L. Du, B. Song, L. Yin, Y. Chen, L. Gao, R. Li, H. Huang, G. Zeng, Antibiotic resistance in soil-plant systems: a review of the source, dissemination, influence factors, and potential exposure risks, Sci. Total Environ. 869 (2023) 161855.
[5] K. Browne, S. Chakraborty, R. Chen, M.D. Willcox, D.S. Black, W.R. Walsh, N. Kumar, A new era of antibiotics: the clinical potential of antimicrobial peptides, Int. J. Mol. Sci. 161855 (2020).
[6] M. Rima, M. Rima, Z. Fajloun, J.M. Sabatier, B. Bechinger, T. Naas, Antimicrobial peptides: a potent alternative to antibiotics, Antibiotics 10 (9) (2021) 1095.
[7] L. Lin, J. Chi, Y. Yan, R. Luo, X. Feng, Y. Zheng, D. Xian, X. Li, G. Quan, D. Liu, et al., Membrane-disruptive peptides/peptidomimetics-based therapeutics: promising systems to combat bacteria and cancer in the drug-resistant era, Acta Pharm. Sin. B 11 (9) (2021) 2609–2644.
[8] S. Ji, F. An, T. Zhang, M. Lou, J. Guo, K. Liu, Y. Zhu, J. Wu, R. Wu, Antimicrobial peptides: an alternative to traditional antibiotics, Eur. J. Med. Chem. 2023 (2023) 116072.
[9] R. Allsopp, A. Pavlova, T. Cline, A.M. Salyapongse, R.E. Gillilan, Y.P. Di, B. Deslouches, J.B. Klauda, J.C. Gumbart, S. Tristram-Nagle, Antimicrobial peptide mechanism studied by scattering-guided molecular dynamics simulation, J. Phys. Chem. B 126 (36) (2022) 6922–6935.
[10] C. Galanth, F. Abbassi, O. Lequin, J. Ayala-Sanmartin, A. Ladram, P. Nicolas, M. Amiche, Mechanism of antibacterial action of Dermaseptin B2: interplay between Helix−hinge−Helix structure and membrane curvature strain, Biochemistry 48 (2) (2009) 313–327.
[11] R.E. Hancock, H.G. Sahl, Antimicrobial and host-defense peptides as new anti-infective therapeutic strategies, Nat. Biotechnol. 24 (12) (2006) 1551–1557.
[12] M. Mahlapuu, C. Björn, J. Ekblom, Antimicrobial peptides as therapeutic agents: opportunities and challenges, Crit. Rev. Biotechnol. 40 (7) (2020) 978–992.
[13] R. Talandashti, F. Mehrnejad, K. Rostamipour, F. Doustdar, A. Lavasanifar, Molecular insights into pore formation mechanism, membrane perturbation, and water permeation by the antimicrobial peptide pleurocidin: a combined all-atom and coarse-grained molecular dynamics simulation study, J. Phys. Chem. B 125 (26) (2021) 7163–7176.
[14] L. Cresti, G. Cappello, A. Pini, Antimicrobial peptides towards clinical application—a long history to be concluded, Int. J. Mol. Sci. 25 (9) (2024) 4870.
[15] L.M. Alec Radford, Soumith Chintala, Unsupervised Representation Learning With Deep Convolutional Generative Adversarial Networks, arXiv preprint, 2015, pp. 20746–20754.
[16] E. Lin, C.H. Lin, H.Y. Lane, De novo peptide and protein design using generative adversarial networks: an update, J. Chem. Inf. Model. 62 (4) (2022) 761–774, https://doi.org/10.1021/acs.jcim.1c01361.
[17] A. Tucs, D.P. Tran, A. Yumoto, Y. Ito, T. Uzawa, K. Tsuda, Generating ampicillin-level antimicrobial peptides with activity-aware generative adversarial networks, ACS Omega 5 (36) (2020) 22847–22851, https://doi.org/10.1021/acsomega.0c02088.
[18] T.T. Lin, L.Y. Yang, C.Y. Lin, C.T. Wang, C.W. Lai, C.F. Ko, Y.H. Shih, S.H. Chen, Intelligent de novo design of novel antimicrobial peptides against antibiotic-resistant bacteria strains, Int. J. Mol. Sci. 24 (7) (2023) 6788.
[19] T.T. Lin, L.Y. Yang, I.H. Lu, W.C. Cheng, Z.R. Hsu, S.H. Chen, C.Y. Lin, AI4AMP: an antimicrobial peptide predictor using physicochemical property-based encoding method and deep, Learning mSystems 6(6) (2021) e0029921.
[20] F.J. Chen, I.W. Huang, C.H. Wang, P.C. Chen, H.Y. Wang, J.F. Lai, T. Hospitals, mecA-positive Staphylococcus aureus with low-level oxacillin MIC in Taiwan, J. Clin. Microbiol. 50 (5) (2012) 1679–1683.
[21] K.Y. Lin, T.L. Lauderdale, J.T. Wang, S.C. Chang, Carbapenem-resistant Pseudomonas aeruginosa in Taiwan: prevalence, risk factors, and impact on outcome of infections, J. Microbiol. Immunol. Infect. 49 (1) (2016) 52–59, https://doi.org/10.1016/j.jmii.2014.01.005.
[22] X. Kang, F. Dong, C. Shi, S. Liu, J. Sun, J. Chen, H. Li, H. Xu, X. Lao, H. Zheng, DRAMP 2.0, an updated data repository of antimicrobial peptides, Scientific data 6 (1) (2019) 148.
[23] F.H. Waghu, R.S. Barai, P. Gurung, S. Idicula-Thomas, CAMPR3: a database on sequences, structures and signatures of antimicrobial peptides, Nucleic Acids Res. 148 (2016).
[24] G. Wang, X. Li, Z. Wang, APD3: the antimicrobial peptide database as a tool for research and education, Nucleic Acids Res. 148 (2016).
[25] X. Zhao, H. Wu, H. Lu, G. Li, Q. Huang, LAMP: a database linking antimicrobial peptides, PLoS One 8 (6) (2013) e66557.
[26] S.N. Dean, S.A. Walper, Variational autoencoder for generation of antimicrobial peptides, ACS Omega 5 (33) (2020) 20746–20754.
[27] Z. Wang, Q. Li, J. Li, L. Shang, J. Li, S. Chou, Y. Lyu, A. Shan, pH-responsive antimicrobial peptide with selective killing activity for bacterial abscess therapy, J. Med. Chem. 65 (7) (2022) 5355–5373.
[28] J.R. Kremer, D.N. Mastronarde, J.R. McIntosh, Computer visualization of three-dimensional image data using IMOD, J. Struct. Biol. 116 (1) (1996) 71–76.
[29] M. Harkiolaki, M.C. Darrow, M.C. Spink, E. Kosior, K. Dent, E. Duke, Cryo-soft X-ray tomography: using soft X-rays to explore the ultrastructure of whole cells, Emerging Topics in Life Sciences 2 (1) (2018) 81–92.
[30] E.M. Duke, M. Razi, A. Weston, P. Guttmann, S. Werner, K. Henzler, G. Schneider, S.A. Tooze, L.M. Collinson, Imaging endosomes and autophagosomes in whole mammalian cells using correlative cryo-fluorescence and cryo-soft X-ray microscopy (cryo-CLXM), Ultramicroscopy 143 (2014) 77–87.
[31] B. Cheng, B. Thapa, K. Remant, P. Xu, Dual secured nano-melittin for the safe and effective eradication of cancer cells, J. Mater. Chem. B 3 (1) (2015) 25–29.
[32] D. Yang, L. Zhu, X. Lin, J. Zhu, Y. Qian, W. Liu, J. Chen, C. Zhou, J. He, Therapeutic effects of synthetic triblock amphiphilic short antimicrobial peptides on human lung adenocarcinoma, Pharmaceutics 14 (5) (2022), https://doi.org/10.3390/pharmaceutics14050929.
[33] S.H. North, C.R. Taitt, Application of circular dichroism for structural analysis of surface-immobilized cecropin a interacting with lipoteichoic acid, Langmuir 31 (39) (2015) 10791–10798, https://doi.org/10.1021/acs.langmuir.5b02600.
[34] O. Lequin, F. Bruston, O. Convert, G. Chassaing, P. Nicolas, Helical structure of dermaseptin B2 in a membrane-mimetic environment, Biochemistry 42 (34) (2003) 10311–10323.
[35] L. Wei, J. Yang, X. He, G. Mo, J. Hong, X. Yan, D. Lin, R. Lai, Structure and function of a potent lipopolysaccharide-binding antimicrobial and anti-inflammatory peptide, J. Med. Chem. 56 (9) (2013) 3546–3556.
[36] M. Aschi, A. Bozzi, C. Luzi, N. Bouchemal, M. Sette, Crabrolin, a natural antimicrobial peptide: structural properties, J. Pept. Sci. 23 (9) (2017) 693–700.

[37] E.M. van Zyl, J.M. Coburn, Functionalization of bacterial cellulose with the antimicrobial peptide KR-12 via chimerical cellulose-binding peptides, Int. J. Mol. Sci. 25 (3) (2024) 1462.
[38] A. Barreto-Santamaría, G. Arévalo-Pinzón, M.A. Patarroyo, M.E. Patarroyo, How to combat gram-negative bacteria using antimicrobial peptides: a challenge or an unattainable goal? Antibiotics 10 (12) (2021) 1499.
[39] C. Avitabile, L.D. D'Andrea, A. Romanelli, Circular dichroism studies on the interactions of antimicrobial peptides with bacterial cells, Sci. Rep. 4 (1) (2014) 4293.
[40] A. Shariati, M. Arshadi, M.A. Khosrojerdi, M. Abedinzadeh, M. Ganjalishahi, A. Maleki, M. Heidary, S. Khoshnood, The resistance mechanisms of bacteria against ciprofloxacin and new approaches for enhancing the efficacy of this antibiotic, Front. Public Health 10 (2022) 1025633.
[41] L. Zhang, M.G. Scott, H. Yan, L.D. Mayer, R.E.W. Hancock, Interaction of Polyphemusin I and structural analogs with bacterial membranes, lipopolysaccharide, and lipid monolayers, Biochemistry 39 (47) (2000) 14504–14514.
[42] A. Cossa, S. Trépout, F. Wien, J. Groen, E. Le Brun, F. Turbant, L. Besse, E. Pereiro, V. Arluison, Cryo soft X-ray tomography to explore Escherichia coli nucleoid remodeling by Hfq master regulator, J. Struct. Biol. 214 (4) (2022) 107912.
[43] S. Yu, B. Jia, Y. Zhang, Y. Yu, Z. Pei, H. Ma, Design, biological characteristics, and antibacterial mechanism of high therapeutic index antimicrobial peptides with PRRP as central axis, J. Antibiot. 2024 (2024) 1–12.
[44] M.Y. Louyeh, M. Sepahi, S. Hadadian, M. Hashemi, Evaluation the therapeutic index of recombinant antimicrobial S3 tetramer-peptides expressed in Ecoli, Int. J. Pept. Res. Ther. 27 (2021) 2439–2447.
[45] S.P. Selvaraj, J.Y. Chen, Conjugation of antimicrobial peptides to enhance therapeutic efficacy, Eur. J. Med. Chem. 2023 (2023) 115680.
[46] S. Singh, H.M. Aldawsari, A. Alam, M.H.S. Alqarni, S. Ranjan, P. Kesharwani, Synthesis and antimicrobial activity of vancomycin–conjugated zinc coordination polymer nanoparticles against methicillin-resistant staphylococcus aureus, Journal of Drug Delivery Science and Technology 70 (2022) 103255.
[47] L. Chalkley, H. Koornhof, Antimicrobial activity of ciprofloxacin against Pseudomonas aeruginosa, Escherichia coli, and Staphylococcus aureus determined by the killing curve method: antibiotic comparisons and synergistic interactions, Antimicrob. Agents Chemother. 28 (2) (1985) 331–342.
[48] Z. Jiang, A.I. Vasil, J. Hale, R.E. Hancock, M.L. Vasil, R.S. Hodges, Effects of net charge and the number of positively charged residues on the biological activity of amphipathic α-helical cationic antimicrobial peptides, in: Peptides for Youth, The Proceedings of the 20th American Peptide Symposium, 2009, pp. 146–150.
[49] M. Dathe, H. Nikolenko, J. Meyer, M. Beyermann, M. Bienert, Optimization of the antimicrobial activity of magainin peptides by modification of charge, FEBS Lett. 501 (2) (2001) 146–150.
[50] J.J. Lopez Cascales, S. Zenak, J. García de La Torre, O.G. Lezama, A. Garro, R. D. Enriz, Small cationic peptides: influence of charge on their antimicrobial activity, ACS Omega 3 (5) (2018) 5390–5398.
[51] Z. Raja, S. André, F. Abbassi, V. Humblot, O. Lequin, T. Bouceba, A. Ladram, Insight into the mechanism of action of temporin-SHa, a new broad-spectrum antiparasitic and antibacterial agent, PLoS One 12 (3) (2017) e0174024.
[52] A. Gholizadeh, B. Moradi, Cecropins activity against bacterial pathogens, Infect. Dis. Clin. Pract. 29 (1) (2021) e6–e12, https://doi.org/10.1097/IPC.0000000000000913.
[53] M.M. Masadeh, A.L.-K. AEA, R. Haddad, M. Alsaggar, K.H. Alzoubi, S.H. Sabi, N. Alrabadi, An antibacterial novel peptide based on cecropin and MAP-27: design and characterization, J. Appl. Pharm. Sci. 13 (3) (2023) 141–152.
[54] W. Chiangjong, S. Chutipongtanate, S. Hongeng, Anticancer peptide: physicochemical property, functional aspect and trend in clinical application (review), Int. J. Oncol. 57 (3) (2020) 678–696, https://doi.org/10.3892/ijo.2020.5099.
[55] L. Lins, R. Brasseur, Tilted peptides: a structural motif involved in protein membrane insertion? J. Pept. Sci. 14 (4) (2008) 416–422, https://doi.org/10.1002/psc.971.